Quasi-elastic Scattering

Arie Bodek* and Howard Budd†

MINERνA Note 100
October, 2004

1 Quasi-Elastic Scattering

1.1 Introduction

Quasi-elastic scattering makes up the largest single component of the total ν–N interaction rate in the threshold regime $E_\nu \leq 2$ GeV. Precision measurement of the cross-section for this reaction, including its energy dependence and variation with target nuclei, is essential to current and future neutrino-oscillation experiments.

1.2 Form-factors in Quasi-elastic Scattering

MINERνA's large quasi-elastic samples will probe the Q^2 response of the weak nucleon current with unprecedented accuracy. The underlying V-A structure of this current include vector and axial-vector form-factors. The essential formalism is given in reference [1].

$$< p(p_2)|J^+_\lambda|n(p_1) >= \overline{u}(p_2)\left[\gamma_\lambda F^1_V(q^2) + \frac{i\sigma_{\lambda\nu}q^\nu \xi F^2_V(q^2)}{2M} + \gamma_\lambda\gamma_5 F_A(q^2)\right] u(p_1), \tag{1}$$

where $q = k_\nu - k_\mu$, $\xi = (\mu_p - 1) - \mu_n$, and $M = (m_p + m_n)/2$. Here, μ_p and μ_n are the proton and neutron magnetic moments. The pseudoscaler form factor is not shown since it is small for ν_μ.

The vector part of this matrix element can be expressed using $G^p_E(q^2)$, $G^n_E(q^2)$, $G^p_M(q^2)$, and $G^n_M(q^2)$. It has been generally assumed that the form-factors q^2

*University of Rochester
†University of Rochester

dependence is described by the dipole approximation.

$$G_D(q^2) = \frac{1}{\left(1 - \frac{q^2}{M_V^2}\right)^2}, \quad M_V^2 = 0.71\ (GeV/c)^2, \quad F_A(q^2) = \frac{g_A}{\left(1 - \frac{q^2}{M_A^2}\right)^2}$$

$$G_E^p = G_D(q^2), \quad G_E^n = 0, \quad G_M^p = \mu_p G_D(q^2), \quad G_M^n = \mu_n G_D(q^2).$$

As discussed below, the dipole parameterization is far from perfect. MINERνA will be able to measure deviations of F_A from this form. In general, the axial form-factor $F_A(q^2)$ can only be extracted from quasi-elastic neutrino scattering. At low q^2 (below 0.1 $(GeV/c)^2$, its behavior can also be inferred from pion electroproduction data.)

1.2.1 Vector Form-factors

Electron scattering experiments at SLAC and Jefferson Lab (JLab) have measured the proton and neutron electromagnetic (vector) form-factors with high precision. The vector form-factors can be determined from electron scattering cross-sections using the standard Rosenbluth separation technique[2], which is sensitive to (two-photon) radiative corrections, or from polarization measurements using the newer polarization transfer technique[3]. Polarization measurements do not directly measure form-factors, but rather the ratio G_E/G_M. Recently, discrepancies in electron scattering measurements of some vector form-factors have appeared; study of quasi-elastic reactions in MINERνA may help reveal the origin these discrepacies. Figure 1 shows the BBA-2003 (Bodek, Budd, Arrington 2003) fits to $G_E^p/dipole$. There appears to be a difference between the two different methods of measuring this ratio. The newer polarization transfer technique yields a much lower value at high Q^2 and indicates a difference between the electric charge and magnetization distributions. The polarization transfer technique is believed to be more reliable and less sensitive to (two-photon) radiative effects from two-photon corrections. In addition, Figure 1 shows that dipole amplitudes provide only a first-order description of form-factor behavior at high Q^2. In general, these deviations are different for each of the form-factors and are shown in reference [4] .

If the electric charge and magnetization distributions of the proton are indeed different, a test of the axial form-factor's high-Q^2 shape can provide important new input to help resolve differences between electron scattering measurements. As discussed below, MINERνA will be able to accurately measure the high-Q^2 behavior of F_A.

To get the correct neutrino cross sections [4], the input form-factors must be correct. The Q^2 distribution as measured in neutrino scattering is sensitive to both the vector and axial form factors. However, using an incorrect axial form factor to match the the Q^2 distribution in neutrino scattering to account for the use

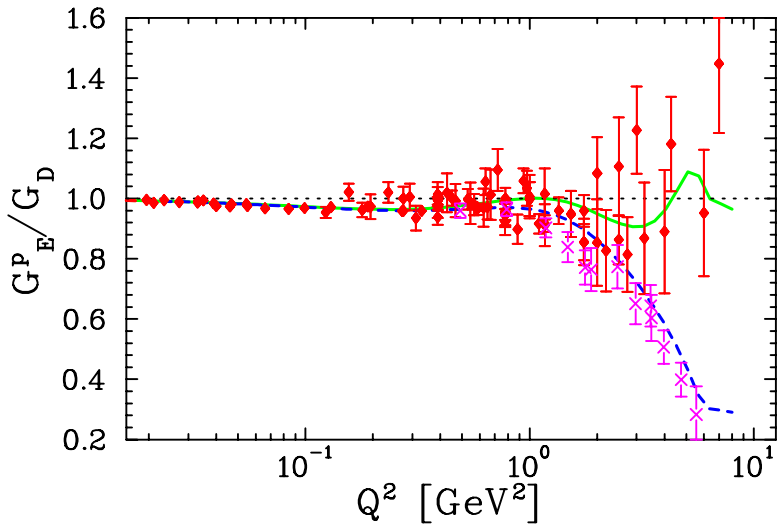

Figure 1: The (BBA-2003) fits to G_E^p/G_D, using cross section data only (solid), and with both the cross section and polarization transfer data (dashed). The diamonds are the from Rosenbluth extractions and the crosses are the Hall A polarization transfer data. Note that Bodek-Budd and Arrington properly do the fit to measured cross sections, rather than fitting directly to the extracted values of the Rosenbluth extracted values of G_E^p shown in the figure.

of incorrect old dipole vector form-factors causes the calculated neutrino cross section to be off by 6-8%. Therefore, one must use both updated vector and better measured axial form factors. MINERνA will measure the Q^2 dependence of F_A in neutrino scattering and compare the calculated cross section with the measured cross section.

1.3 Axial Form-factor of the Nucleon

Neutrino scattering provides the only practical route to precision measurement of the axial form-factor above $Q^2 = 0$ and the functional form of $F_A(Q^2)$. The fall-off of the form-factor strength with increasing Q^2 is traditionally parameterized (approximately) using an effective axial-vector mass M_A. Uncertainty in the value of M_A contributes directly to uncertainty in the total quasi-elastic cross-section. Earlier neutrino measurements, mostly bubble-chamber experiments on deuterium, extracted M_A using the best vector form factors and inputs and models available at the time. Changing these input assumptions changes the extracted value of M_A. Hence, precision extractions of M_A and F_A require using the best possible vector form-factors and coupling constants. The value of M_A is ≈ 1.00 GeV$/c^2$ to an accuracy of perhaps 5%. This value agrees with the theoretically-corrected value from pion electroproduction[5], 1.014 ± 0.016 GeV$/c^2$.

The fractional contributions of F_A, G_M^p, G_M^n, G_E^p, and G_E^n to the Q^2 distribu-

tion for quasi-elastic neutrino and anti-neutrino scattering cross sections in energy range of the NuMI beam are shown in Figure 2. The contributions are determined by comparing the BBA-2003 cross-sections with and without each of the form-factors included. MINERνA will be the first systematic study of F_A, which accounts for roughly half of the quasi-elastic cross-section, over the entire range of Q^2 shown in the figure.

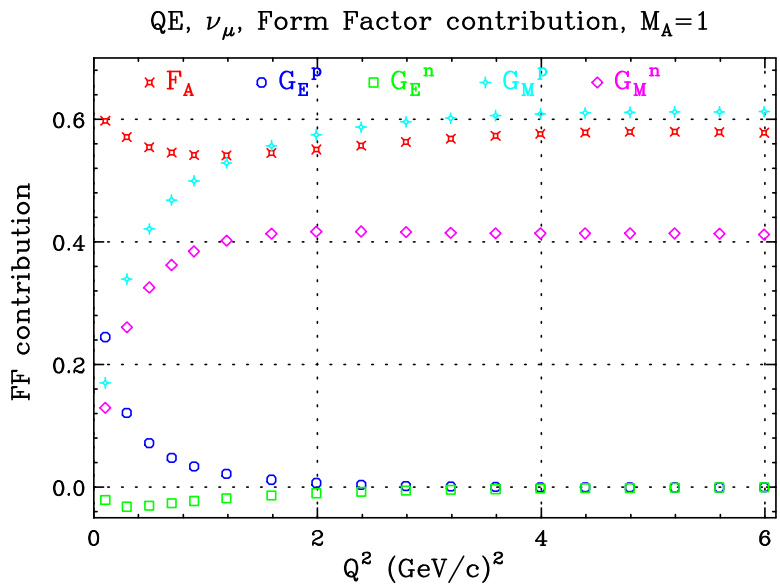

Figure 2: Fractional contributions of G_M^p, G_M^n, G_E^p, G_E^n, and F_A to the Q^2 distributions for quasi-elastic neutrino samples in the energy range of the NuMI beam. Because of interference terms, the sum of the fractions does not necessarily add up to 100%.

1.3.1 Physics of Vector and Axial Form Factors

In deep inelastic charged current scattering from quarks, the vector and axial couplings are equal (V-A). Similarly, in electron scattering from quarks (vector current), there is a well defined ratio between electric and magnetic scattering from point-like dirac quarks. At low momentum transfers, all of these relations break down. For example in quasielastic and resonance production at very low momentum transfers, the charge and anomalous magnetic moments of the neutron and proton means that the ratio of electric and magnetic scattering for the vector current is not the same as it is for free quarks. Similarly, from neutron decay, we know that $g_a(Q^2 = 0) = 1.267$ instead of 1.0, so vector and axial scattering are not equal at Q^2=0.

There are current efforts by lattice gauge programs to calculated the anomalous vector and axial magnetic moments of the proton and neutron and the Q^2

dependence of all the form factors both the low and high Q^2 regions. The normalization of the magnetic form factors at Q^2=0 are constrained to be equal to the charge and anomalous (vector and axial) magnetic moment. The slope at low Q^2 is related to the mean square charge radius of the proton and neutron. The dipole form assumes that the charge and magnetization distributions of the various types of quarks and antiquarks have an exponential form. For Q^2 above 0.5-1.0 $(GeV/c)^2$ this non-relativistic picture breaks down. The fact that the ratio $Ge/\mu Gm$ is 1.0 at low Q^2 implies that the charge and magnetization distribution of the proton are the same. The fact at at higher Q^2 the ratio becomes much smaller implies that this picture breaks down, and more sophisticated models need to be used (e.g. lattice gauge theories etc.). Therefore, a measurement of the axial form factor over a wide range of Q^2 is of great interest. In this section, we show the sensitivity of the MINERvA experiment to three different models of the axial form factor:

(1) Model 1: A simple dipole as is currently used for the magnetic form factor of the proton (except for the fact that the axial and vector radii are different). This is the current standard assumption.

(2) Model 2: A model in which the ratio to the dipole of the axial form factor is the same as the ratio to dipole of the electric form factor of the proton and goes down with Q^2.

(3) Model 3: A model based on duality, which requires the axial and vector parts for $W_1^{elastic}$ to be equal above Q^2=0.5 $(GeV/c)^2$, and therefore increases with Q^2, as described briefly in the next section.

1.3.2 Quark-Hadron and local Duality

In modern language, the concept of quark-hadron duality can related to the momentum sum rule in QCD, and various other moments of the structure functions. It has been shown by Bodek and Yang that with the inclusion of target mass corrections, NNLO QCD describes DIS and the average of resonance data all the way down to Q^2=0.5 $(GeV/c)^2$. The concept of local duality implies that the integral of the QCD predictions (including target mass) in the threshold region up to pion threshold, should be equal to the integral of the elastic peak. Therefore, since for QCD, the vector and axial contributions to W_1 and W_2 are equal, local duality predicts that vector and axial part of the quasielastic form factors should become equal around Q^2=0.5 $(GeV/c)^2$. This means that the dipole form must break down for both vector and axial form factors.

The vector and axial components of $W_1^{elastic}$ become equal at $Q^2 \sim 0.5\ (GeV/c)^2$ for both BBA-form factors and dipole form factors. The requirement that this ratio of vector/axial remains equal to 1.0 for higher Q^2 yields a definite prediction that the axial form factor is a factor of 1.4 times the dipole prediction at higher Q^2.

1.3.3 Measurement of the axial form-factor in MINERνA

Figure 3 shows a typical quasi-elastic event, as simulated in MINERνA.

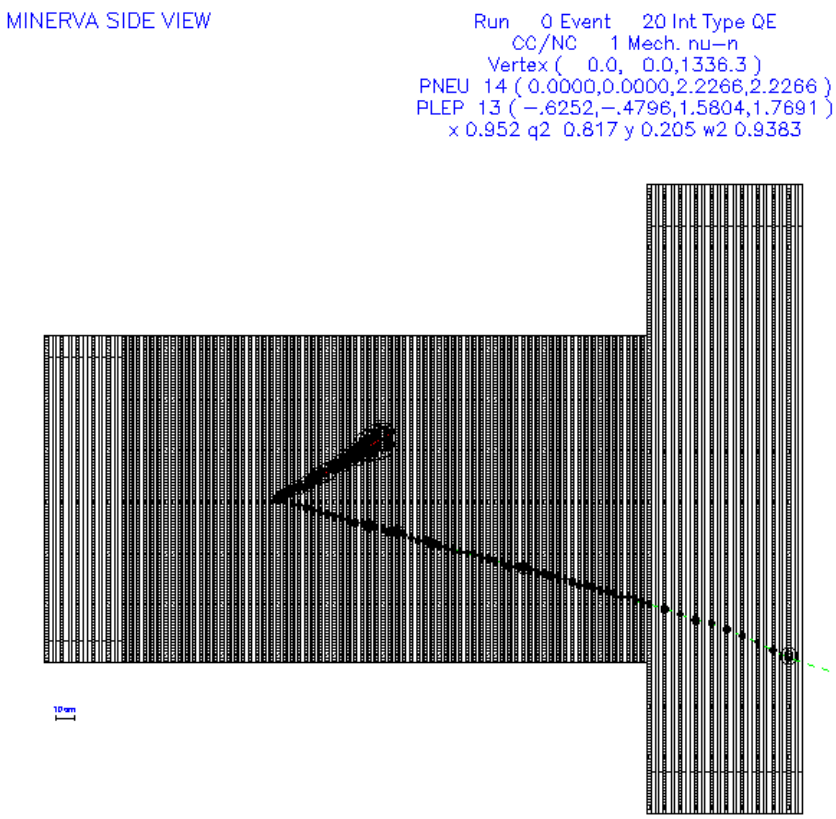

Figure 3: A simulated charged-current quasi-elastic interaction in MINERνA. The proton (upper) and muon (lower) tracks are well resolved. In this display, hit size is proportional to energy loss within a strip. The increased energy loss of the proton as it slows and stops is clear. Note that for clarity the outer detector has not been drawn.

In $\nu n \rightarrow \mu^- p$, the outgoing proton carries a kinetic energy that is approximately $Q^2/2M_N$. So for low Q^2, the challenge is identifying events with a very soft recoil proton; for high Q^2, this proton is high energy and may interact in the detector, making particle identification more challenging. The main strategies of the current analysis are:

- At low Q^2, accept quasi-elastic candidates with a single (muon) track, and discriminate from background by requiring low activity in the remainder of the detector
- At higher Q^2, reconstruct both the proton and the muon, and require kinematic consistency with $x = 1$ and $p_T = 0$

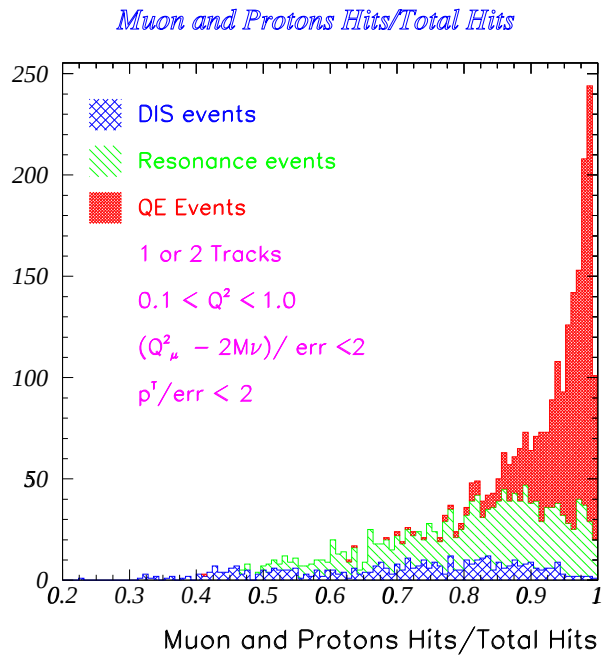

Figure 4: The fraction of hits associated with the muon and the proton tracks in quasi-elastic candidates. The events for the plot may have have one or two vertex tracks, pass additional kinematic requirement and are required to have $0.1\ (GeV/c)^2 < Q^2 < 1\ GeV^2$.

Simple cuts deriving from these ideas allow for reasonable efficiency with good purity, even at high Q^2.

The analysis described her uses the NEUGEN generation and the hit level MINERνA simulation and tracking package in order to simulate signal selection and background processes.

The initial event identification proceeds by requiring one or two tracks in the active target. One of these tracks must be long range (400 g/cm^2) as expected from a muon. If a second track forms a vertex with this track, it is assumed to be the proton. No other tracks are allowed to be connected with this event vertex. The muon track momentum is reconstructed with a fractional uncertainty of between 10–20%.

In the low Q^2 case, the proton track (if found) would be effectively required to lose energy by range since only a limited amount of detector activity not associated with the primary tracks is allowed by the event selection. We attempt to recover some of the lost efficiency at higher Q^2 due to this cut by allowing hits on tracks near the proton track to be associated with the proton track itself. Figure 4 shows the fraction of hits not associated with the lepton or proton in the quasi-elastic events and in expected background processes. For higher Q^2 events a similar requirement could in principle be applied, but it is not particularly effective

nor efficient.

The energy of the proton for the high Q^2 case (where the proton almost always interacts) is reconstructed calorimetrically with an expected fractional energy resolution that is well parameterized by $35\%/\sqrt{E_{proton}}$.

Although muons are identified by requiring a single track with a long range in the detector, no attempt was made (in this initial analysis) to improve particle identification by requiring a dE/dx consistent with the muon or proton tracks. This requirement is expected to be particularly effective for protons of $\mathcal{O}(1)$ GeV momentum[1], and such a requirement can be optimized to improve the analysis in the future. In addition, it may be possible to improve the efficiency by allowing a lower range muon with a dE/dx requirement without sacrificing purity.

If a quasi-elastic interaction is assumed, one can reconstruct the event kinematics from only the momentum and direction of the final state μ. Neglecting the binding energy of the final state proton,

$$E_\nu^{QE} = \frac{M_N E_\mu - \frac{m_\mu^2}{2}}{M_N - E_\mu + p_\mu \cos\theta_\mu}.$$

If a proton track is required and its angle and energy are measured, one can additionally require consistency with the quasi-elastic hypothesis. Two constraints are possible, one on the x of the reconstructed interaction and one on the p_T of the observed final state.

If the interaction is truly quasi-elastic, then $x = 1$, and therefore $Q^2 = 2M_N\nu$ where ν = E_{had} - $M_{nucleon}$, and E_{had} is the energy of the hadronic final state. In this analysis, we test this by comparing Q^2 reconstructed from the lepton kinematics under the quasi-elastic hypothesis to $2M_N\nu$ and forming $(Q_\mu^2 - 2M_N\nu)/error$ where the dominant part of the calculated error for this term comes from the smearing of hadronic final state energy. Figure 5 shows this Q^2 difference significance for two track quasi-elastic candidates with observed $1\ (GeV/c)^2 < Q^2 < 3\ (GeV/c)^2$, for quasi-elastic, resonance and DIS events. Note that this cut can be applied without identifying a proton track if the visible energy, less the muon energy, is assumed to be ν.

The Q^2 significance (x) cut does not use information on the proton direction, and so we impose a second kinematic cut on the p^T of the final state relative to the incoming neutrino direction. This selection requires that a proton track is identified and we cut on the significance of the difference from $p_T = 0$. We impose a cut of $p^T/error$ <2 except for $Q^2 > 3\ (GeV/c)^2$, for which the cut is 3. Note also that if we impose a p^T cut first, the Q^2 difference cut still improves the result, i.e. both cuts are needed.

In summary, the selection requirements for quasi-elastic candidates are:

- One or two tracks for $Q^2 < 1\ (GeV/c)^2$ and two tracks for $Q^2 > 1\ GeV^2$.

[1]see Section 15.5.5 of the main proposal

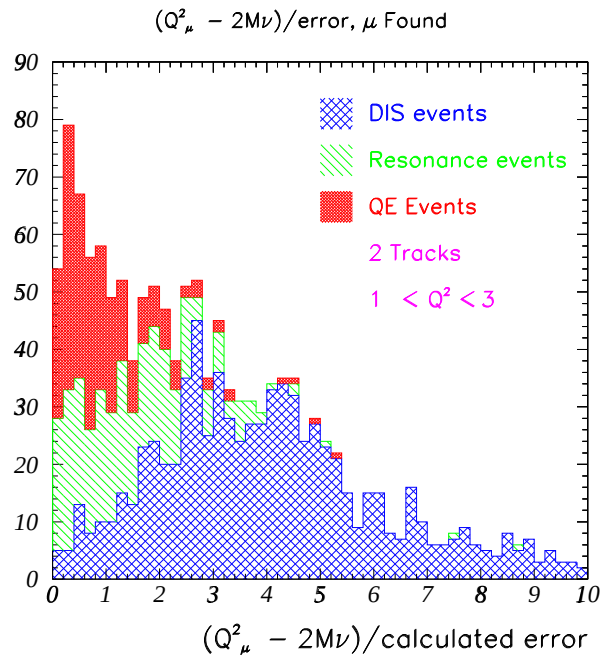

Figure 5: The significance of the difference between Q^2 from the quasi-elastic hypothesis and Q^2 from the final state energy

- One track must have 400 g/cm^2 range (muon).
- $(Q^2_\mu - 2M\nu)/(error) < 2$.
- $p_T/(error) < 2$ for $Q^2 < 3\ (GeV/c)^2$ and $p_T/(error) < 3$ for $Q^2 > 3\ (GeV/c)^2$.
- Hit fraction associated with muon and proton > 0.9, for $Q^2 < 0.5\ (GeV/c)^2$, or > 0.85, for $0.5\ GeV^2 < Q^2 < 1.0\ GeV^2$.

1.3.4 Results

Table 1 shows the efficiency and purity of the quasi-elastic sample for different Q^2 bins after each cut. Using these efficiency and purity, we have determined uncertainties on F_A to include efficiency or background effects.

Figure 6 shows predictions for the cross section assuming the BBA-2003 Form-factors, with the M_A = 1.00 $(GeV/c)^2$. The predicted MINERνA points are shown along with their expected errors. The MIPP experiment will be measuring the particle production off the MINOS target. From this, we expect an additional overall error of 4% from the flux. Figures 6 summarize current knowledge of neutrino quasi-elastic cross-sections. Among the results shown, there are typically 10–20% normalization uncertainties from knowledge of the fluxes. This

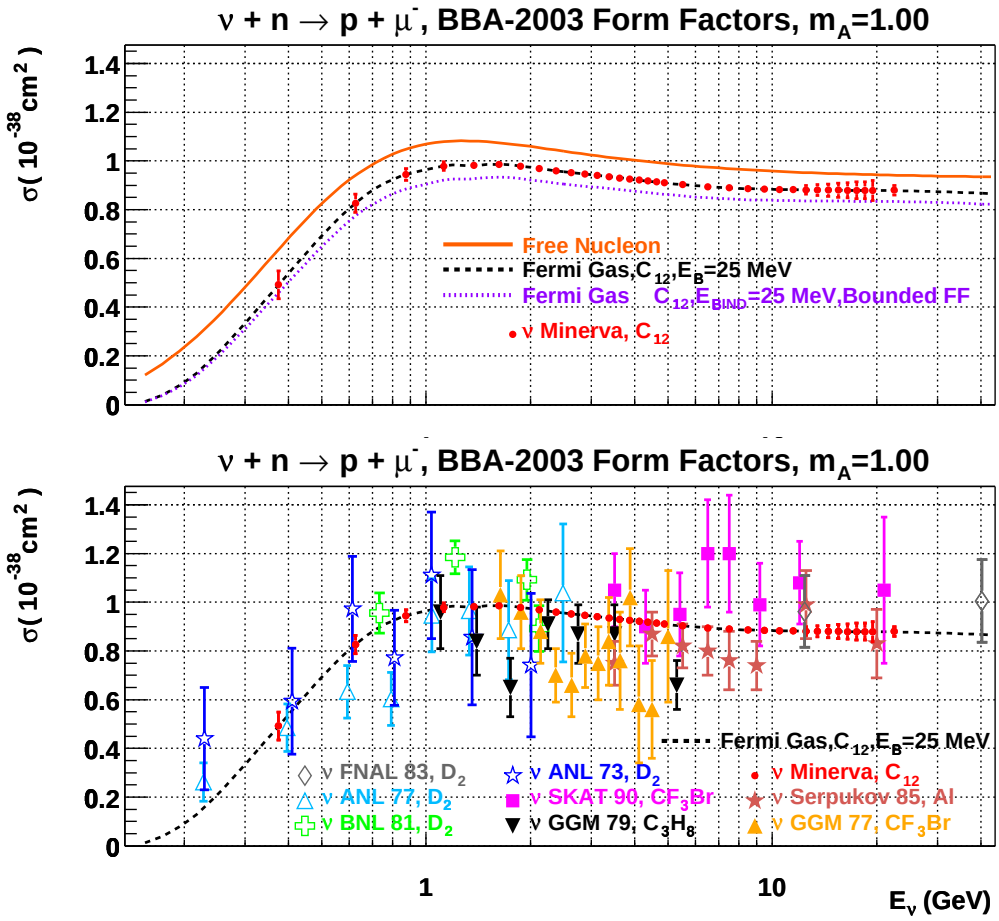

Figure 6: The QE neutrino cross section along with data from various experiments. Representative calculations are shown using BBA-2003 form factors with $M_A = 1.00\,\mathrm{GeV}/c^2$. The solid curve uses no nuclear correction, while the dashed curve [6] uses a Fermi gas model for carbon with a 25 MeV binding energy and 220 Fermi momentum. The dotted curve is the prediction for carbon including both Fermi gas Pauli blocking and the effect of nuclear binding on the nucleon form factors [7](bounded form factors). The predicted MINERνA points are shown. The data shown in the bottom plot are from FNAL 1983 [8], ANL 1977 [9], BNL 1981 [10], ANL 1973 [11], SKAT 1990 [12], GGM 1979 [13], LSND 2002 [14], Serpukov 1985 [15], and GGM 1977 [16]. The data have large errors and are only marginally consistent throughout the E_ν range.

	μ		$(Q^2_\mu - 2M\nu)$/err		p_T /err		Hits	
Q^2 bin	Effic	Purity	Effic	Purity	Effic	Purity	Effic	Purity
0.1-0.5	0.926	0.246	0.918	0.442	0.866	0.559	0.775	0.842
0.5 - 1	0.775	0.199	0.765	0.410	0.624	0.486	0.528	0.685
1 - 2	0.600	0.199	0.541	0.416	0.397	0.555	0.338	0.598
2 - 3	0.456	0.146	0.400	0.375	0.344	0.554	0.278	0.676
3 - 10	0.689	0.123	0.600	0.310	0.467	0.420	0.311	0.700

Table 1: Efficiency and purity in Q^2 bins for quasi-elastic candidates

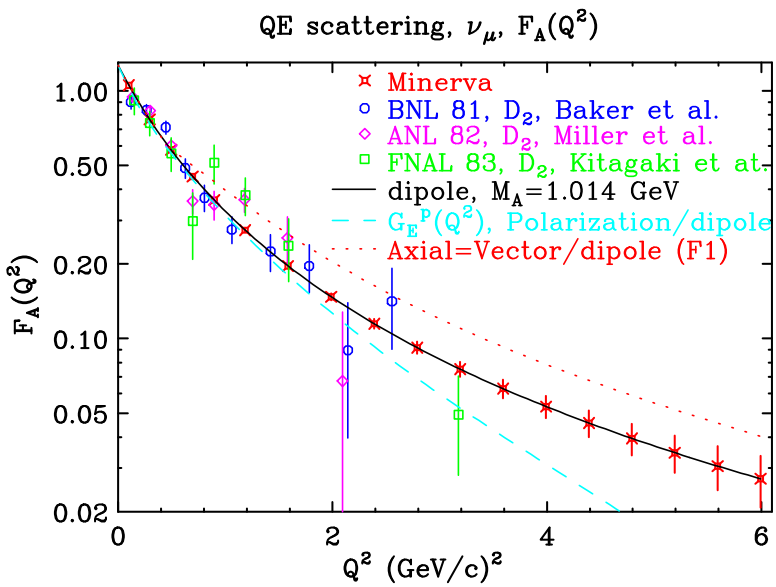

Figure 7: Estimation of F_A from a sample of Monte Carlo neutrino quasi-elastic events recorded in the MINERνA active carbon target. Here, a pure dipole form for F_A is assumed, with $M_A = 1.014$ GeV$/c^2$. The simulated sample and error bars correspond to four years of NuMI running. Also shown is F_A extracted from deuterium bubble chamber experiments using the $d\sigma/dq^2$ from the papers of FNAL 1983 [8] BNL 1981 [10], and ANL 1982 [17]. Also shown is the expectations from Model 2 (dashed line) and Model 3 (dotted line) for the axial form factor.

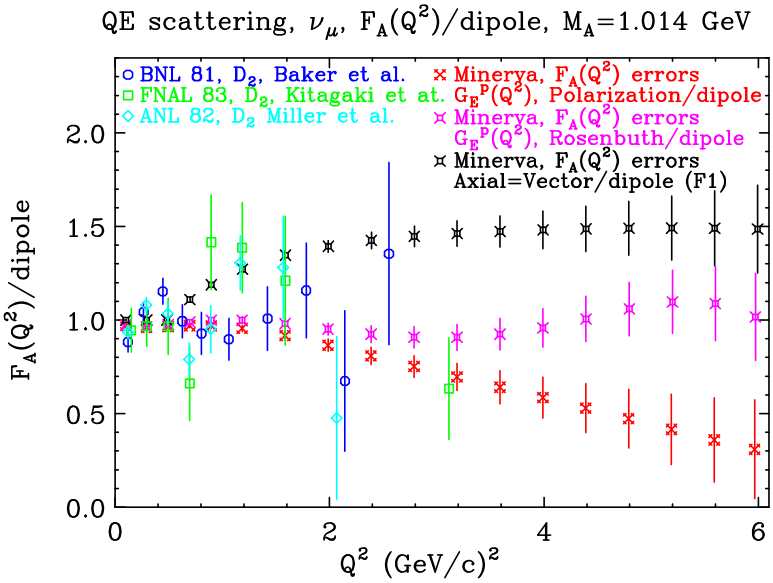

Figure 8: Extracted values of $F_A(q^2)/dipole$ for deuterium bubble chamber experiments Baker *et al.* [10], Miller *et al.* [17], and Kitagaki *et al.* [8]. For MINERνA the projected results are shown for three different assumptions: F_A/dipole=G_E^p/dipole from cross section (model 1), F_A/dipole=G_E^p/dipole from polarization (model 2) and the expectation from the model based on duality (model 3). The MINERνA errors are for a 4 year run.

plot shows that existing measurements have large errors throughout the E_ν range accessible to MINERνA and especially in the threshold regime which is crucial to future oscillation experiments.

Figure 7 shows the expected values and errors of F_A in bins of Q^2 for the MINERνA active carbon target, for a four-year exposure in the NuMI beam. The method to extract F_A from $d\sigma/dq^2$ is given in reference [19]. Clearly the high-Q^2 regime, which is inaccessible to K2K, MinibooNE and J-PARCnu, will be well-resolved in MINERνA. Figure 8 show these results as a ratio of F_A/F_A(Dipole), demonstrating MINERνA's ability to distinguish between different models of F_A. We show the three different models (described earlier) for F_A as a function of Q^2 . Model 2 is a factor of 5 lower at high Q^2, as indicated by G_E^p/G_M^p data, model 3 (based on duality is a factor of 1.4 higher. MINERνA will be able to measure the axial nucleon form-factor with precision comparable to vector form-factor measurements at JLab. Note that resolution effects are still not included in this extraction of F_A; however, the typical Q^2 resolution for quasi-elastic events at high Q^2 is $\lesssim 0.2\ (GeV/c)^2$ which is smaller than the bin size.

Figure 7 and 8 shows the extraction of F_A from Miller, Baker, and Kitagaki, using their plots of $d\sigma/dq^2$. Figure 8 shows that for $Q^2 > 2\ (GeV/c)^2$ there is essentially no measurement of F_A. Even the measurements of F_A of Q^2 below $2\ (GeV/c)^2$ have significant error, hence one cannot assume F_A is a dipole for low Q^2. The maximum Q^2 values that can be achieved with incident neutrino energies of 0.5, 1.0, 1.5 and 2 GeV are 0.5, 1.2, 2.1 and 3.0 (GeV/c)^2, respectively. Since K2K, MiniBooNE, and J-PARCnu energies are in the 0.7–1.0 GeV range, these experiments probe the low $Q^2 < 1$ (GeV/c)^2 region where nuclear effects are large (see Figures 9 and 11). The low Q^2 ($Q^2 < 1$ (GeV/c)^2) MiniBooNE and K2K experiments have begun to investigate the various nuclear effects in carbon and oxygen. However, the higher Q^2 data are only accessible in higher-energy experiments like MINERνA, which can span the 2–8 GeV neutrino energy range. MINERνA's measurement of the axial form-factor at high Q^2 will be essential to a complete understanding of the vector and axial structure of the neutron and proton.

1.4 Nuclear Effects in Quasi-elastic Scattering

1.4.1 Fermi gas model

There are three important nuclear effects in quasi-elastic scattering from nuclear targets: Fermi motion, Pauli blocking, and corrections to the nucleon form-factors due to distortion of the nucleon's size and its pion cloud in the nucleus. Figure 9 shows the nuclear suppression versus E_ν from a NUANCE[20] calculation[6] using the Smith and Moniz[21] Fermi gas model for carbon. This nuclear model includes Pauli blocking and Fermi motion but not final state interactions. The Fermi gas model uses a nuclear binding energy $\epsilon = 25$ MeV and Fermi momen-

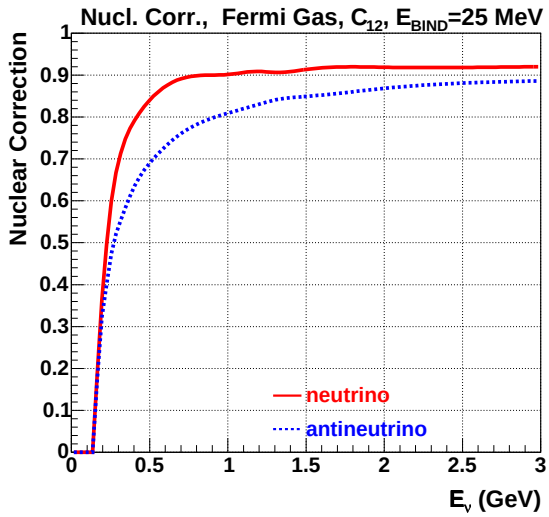

Figure 9: Pauli suppression in a Fermi gas model for carbon with binding energy $\epsilon = 25$ MeV and Fermi momentum $k_f = 220$ MeV/c. A similar suppression is expected for quasi-elastic reactions in MINERνA.

tum $k_f = 220$ MeV/c. Figure 10 from Moniz et. al.[21] shows how the effective k_f and nuclear potential binding energy ϵ (within a Fermi-gas model) for various nuclei is determined from electron scattering data. The effective k_f is extracted from the width of the scattered electron energy distribution, and the binding energy ϵ from the shifted location of the quasi-elastic peak.

1.4.2 Bound nucleon form-factors

The predicted distortions of nucleon form-factors due to nuclear binding are shown in Figure 11 as the ratios of F_1, F_2, and F_A for bound and free nucleons. With a variety of nuclear targets, MINERνA will be able to compare measured form-factors for a range from light to heavy nuclei. Figure 6 shows the suppression of the cross section due to bound form factors. Figure 1.4.2 shows $d\sigma/dq^2$ for an energies that are designed to simulate Miniboone and K2K. The plot shows the suppression at low Q^2 due to the bounded form factors.

Also shown on Figure 1.4.2 is the effect of requiring the vector and axial contributions for W_1 to be equal for $Q^2 > 0.5\ (GeV/c)^2$. As shown on the plot this gives another suppression of low Q^2 relative to high Q^2. Figure 1.4.2 also shows the ratio of $d\sigma/dq^2$ for the various assumptions to $d\sigma/dq^2$ calculated with dipole form form factors.

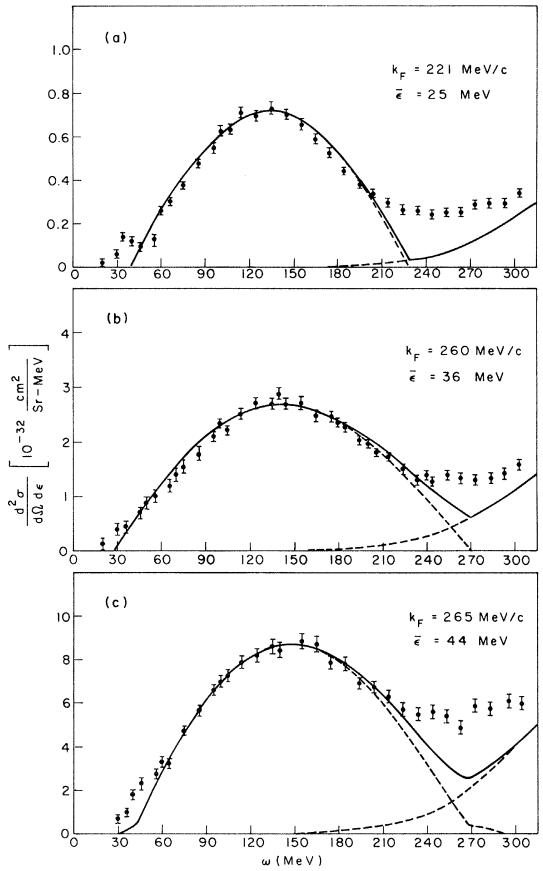

Figure 10: Extraction of Fermi gas model parameters, the effective Fermi momentum k_f and nuclear binding energy ϵ, from 500 MeV electron scattering data[21]. Distributions shown correspond to scattering from (a) carbon, (b) Nickel, and (c) Lead.

1.4.3 Intra-nuclear rescattering

In neutrino experiments, detection of the recoil nucleon helps distinguish quasi-elastic scattering from inelastic reactions. Knowledge of the probability for outgoing protons to reinteract with the target remnant is therefore highly desirable. Similarly, quasi-elastic scattering with nucleons in the high-momentum tail of the nuclear spectral function needs to be understood. More sophisticated treatments than the simple Fermi gas model are required. Conversely, inelastic reactions may be misidentified as quasi-elastic if a final-state pion is absorbed in the nucleus. Because of its constrained kinematics, low-energy neutrino-oscillation experiments use the quasi-elastic channel to measure the (oscillated) neutrino energy spectrum at the far detector; the uncertainty in estimation of this background due to proton intra-nuclear rescattering is currently an important source of systematic error in the K2K experiment.

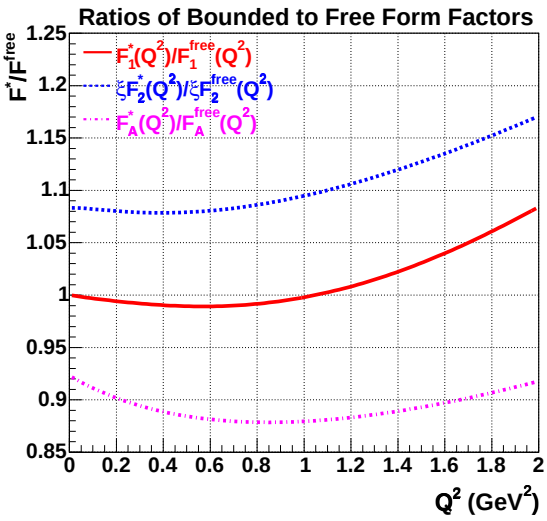

Figure 11: The ratio of bound (in carbon) to free nucleon form-factors for F_1, F_2, and F_A from Ref [7]. Binding effects on the form-factors are expected to be small at higher Q^2 (therefore, this model is not valid for $Q^2 > 1$ (GeV/c)^2).

The best way to study these effects is to analyze electron scattering on nuclear targets (including the hadronic final states) and test the effects of the experimental cuts on the final-state nucleons. MINERνA can address proton intra-nuclear rescattering by comparing nuclear binding effects in neutrino scattering on carbon to electron data in similar kinematic regions. Indeed, MINERνA members will be working with the CLAS collaboration to study hadronic final states in electron scattering on nuclear targets using existing JLab Hall B data. This analysis will allow theoretical models used in both electron and neutrino experiments to be tested. Other work in progress, with the Ghent[22] nuclear physics group, will develop the theoretical tools needed to extract the axial form-factor of the nucleon using MINERνA quasi-elastic data on carbon. The ultimate aim is to perform nearly identical analyses on both neutrino and electron scattering data in the same range of Q^2.

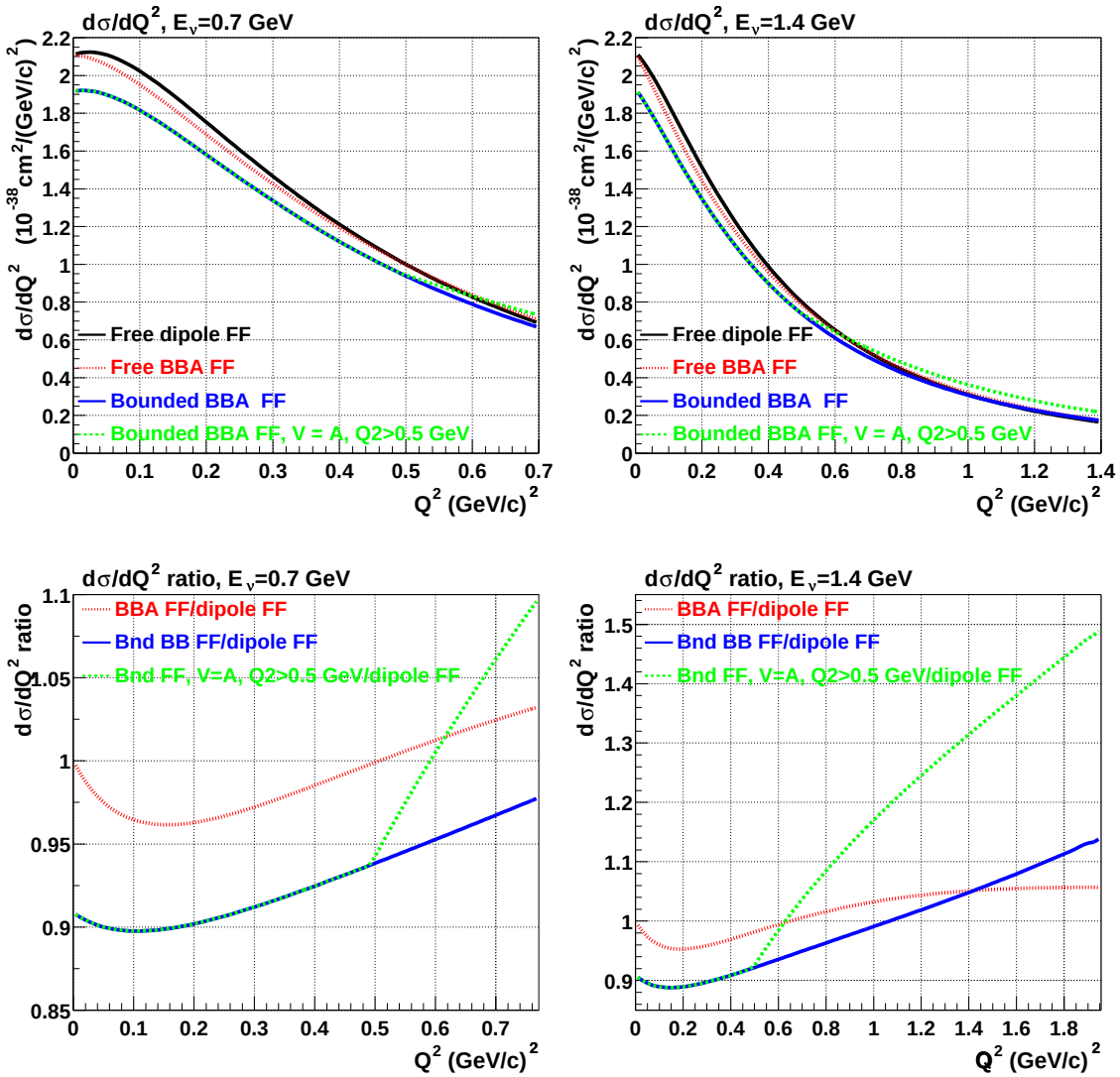

Figure 12: $d\sigma/dq^2$ assuming various models of form factors. We use M_A=1.014 GeV/c^2

. The curve labeled "Free dipole FF" has no correction to dipole form Factors. "Free BBA FF" has no correction to BBA-Form Factors. "Bounded FF" puts in the binding effects on the form factors from ref [7]. "Bounded FF, V=A" shows the duality prediction with Bounded form factors. The top set of plots shows $d\sigma/dq^2$, while the bottom set of plots shows the ratio of $d\sigma/dq^2$ to $d\sigma/dq^2$ with dipole free form factors. The Q^2 upper limit on the plot is the kinematic limit.

References

[1] C.H. Llewellyn Smith, Phys. Rep. **3C** (1972).

[2] J. Arrington, nucl-ex/0305009.

[3] M. K. Jones *et al.*, Phys. Rev. Lett **84**, 1398 (2000); O. Gayou *et al.*, Phys. Rev. Lett **88**, 092301 (2002).

[4] H. Budd, A. Bodek and J. Arrington, To be published in *Proceedings of the Second Workshop on Neutrino-Nucleus Interactions in the Few-GeV Region (NUINT02)*, Irvine, California (2002), arXiv:hep-ex/0308005.

[5] V. Bernard, L. Elouadrhiri, U.G. Meissner, J. Phys. **G28** (2002).

[6] G. Zeller (private communication).

[7] K. Tsushima, Hungchong Kim, K. Saito, nucl-th[0307013].

[8] T. Kitagaki *et al.*, Phys. Rev. **D26**, 436 (1983).

[9] S. J. Barish *et al.*, Phys. Rev. **D16**, 3103 (1977).

[10] N. J. Baker *et al.*, Phys. Rev. **D23**, 2499 (1981).

[11] W.A. Mann *et al.*, Phys. Rev. Lett. **31**, 844 (1973).

[12] J. Brunner *et al.*, Z. Phys. **C45**, 551 (1990).

[13] M. Pohl *et al.*, Lett. Nuovo Cimento **26**, 332 (1979).

[14] L.B. Auerbach *et al.*, Phys. Rev. **C66**, 015501 (2002).

[15] S.V. Belikov *et al.*, Z. Phys. **A320**, 625 (1985).

[16] S. Bonetti *et al.*, Nuovo Cimento **38**, 260 (1977)

[17] K.L. Miller *et al.*, Phys. Rev. **D26** (1982) 537.

[18] H. Budd, A. Bodek and J. Arrington, [arXiv:hep-ex/0308005]; A. Bodek, H. Budd and J. Arrington, [arXiv:hep-ex/0309024] (to be published in Proceedings of CIPANP2003, New York City, NY 2003.)

[19] H. Budd, A. Bodek and J. Arrington, To be published in *Proceedings of the Third Workshop on Neutrino-Nucleus Interactions in the Few-GeV Region (NUINT04)*, Laboratori Nazionali del Gran Sasso - INFN - Assergi(2004), arXiv:hep-ex/0410055.

[20] D. Casper, Nucl. Phys. Proc. Suppl. **112**, 161 (2002).

[21] R. A. Smith and E. J. Moniz, Nucl. Phys. **B43**, 605 (1972) ; E. J. Moniz *et al.*, Phys. Rev. Lett. **26**, 445 (1971); E. J. Moniz, Phys. Rev. **184**, 1154 (1969).

[22] Ghent Theory group in Belgium, Jan Ryckebusch (jan@inwpent5.UGent.be).